Supplementary file to the submission:
A multi-fidelity data-driven model for highly accurate and computationally efficient modeling of short fiber composites

Hon Lam Cheung[1] and Mohsen Mirkhalaf[2*]

[1]Department of Mechanics and Maritime Sciences, Chalmers University of Technology, Hörsalsvägen 7A, Gothenburg, 412 96, Sweden.
[2*]Department of Physics, University of Gothenburg, Origovägen 6B, Gothenburg, 412 96, Sweden.

*Corresponding author(s). E-mail(s): mohsen.mirkhalaf@physics.gu.se;

1 Results

1.1 Test set result

The test is conducted following the test procedure and the results are presented in Table 1.

Table 1: Mean relative error (MeRE) and maximum relative error (MaRE) results for the test data set.

	Average MeRE	Average MaRE
Original	0.0943	0.2005
From Scratch	0.0659	0.1378
Fine-tuned	0.0312	0.0675

2 Data generation

2.1 Constitutive properties of the composite constituents

Constitutive properties of fiber and matrix materials, used in this study, are listed in Table 2.

Table 2: Constitutive properties of elasto-plastic matrix and elastic fibers.

Fiber properties		**Matrix properties**	
Young's modulus	76 GPa	Young's modulus	3.1 GPa
Poisson's ratio	0.22	Poisson's ratio	0.35
Length	240 μm	Yield strength	25 MPa
Diameter	10 μm	Linear hardening modulus	150 MPa
Fiber volume fraction	0.1-0.15	Hardening modulus	20 MPa
		Hardening exponent	325

2.2 Representative Volume Element (RVE) size determination

Figure 1 displays examples of Uni-Directional (UD), planar, and 3D fiber orientation RVEs and respective sizes in different directions. The RVE's dimensions are chosen based on fiber length and diameter, and are indicated with different arrows in different directions.

2.2.1 Uni-directional fiber orientation case

For the uni-directional fiber orientation case, different sizes of micro-structural samples were examined. These sizes were chosen with respect to the fiber dimensions. Specifically, the sizes were chosen as 2, 3, and 4 times the fiber length in the fiber longitudinal direction, and 4, 5, and 6 times the fiber diameter in the transverse direction. The mentioned sizes are referred to as 2L4D, 3L5D, and 4L6D, respectively. Four realizations were generated for each size and the properties for each realization are listed in Table 3. For each realization, 4 monotonic uni-axial stress loading cases (with strain

Table 3: List of UD fiber orientation sample properties.

Size	**Sample**	a_{11}	a_{22}	a_{33}	a_{12}	a_{13}	a_{23}	v_f
2L4D	#1, 2, 3, 4	1	0	0	0	0	0	0.1227
3L5D	#1, 2, 3, 4	1	0	0	0	0	0	0.1361
4L6D	#1, 2, 3, 4	1	0	0	0	0	0	0.1309

range of 0 to 0.05) were tested, namely σ_{11}, σ_{22}, σ_{12} and σ_{23}. The normal stress components demonstrated a higher discrepancy between different realizations, and therefore, the following part focuses on the normal stress results. Figure 2 displays the average response with bounds of standard deviation, and the coefficient of variation results for uni-axial stress loading in σ_{11} and σ_{22}. Since all fibers are orientated towards and

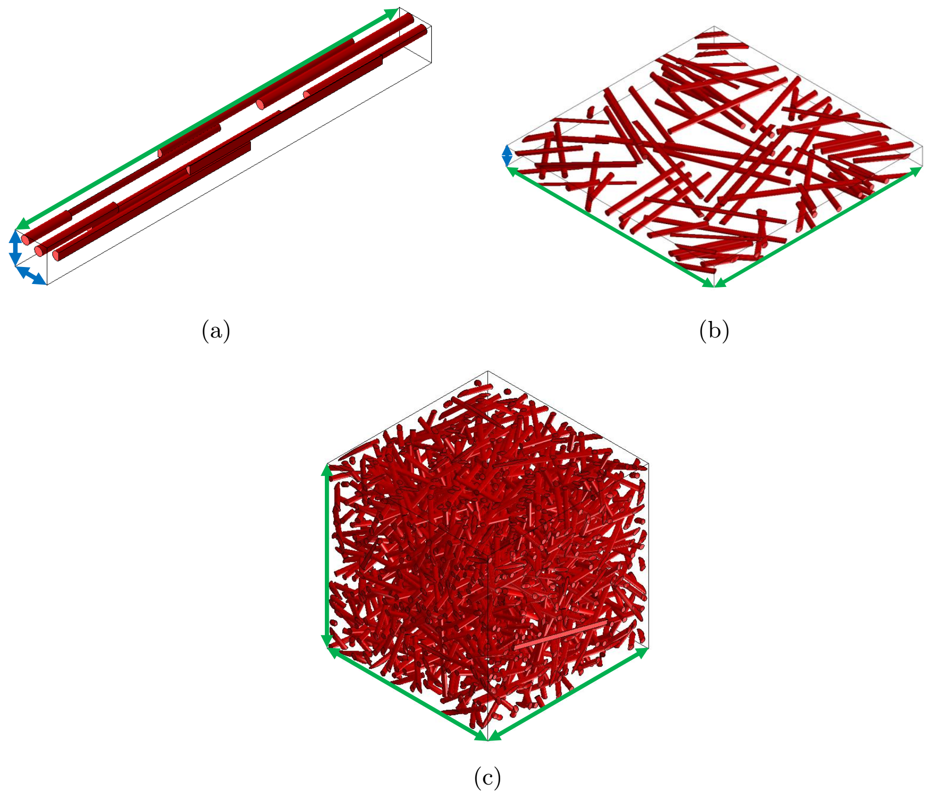

Fig. 1: Represenation of (a) uni-directional, (b) planar, and (c) 3D fiber orientation RVEs.

reinforcing the x-direction, the stress component σ_{11} is considerably higher than σ_{22}. Consequently, the variation in σ_{11} is also higher compared to σ_{22}. However, the σ_{11} variation for all three sizes of micro-structural samples remains below 7%, and below approximately 4% for 4L6D. And Figure 3 illustrates the absolute percentage change in average stress when comparing a smaller RVE size to a larger RVE size. The highest change is observed for σ_{11} when comparing 2L4D and 3L5D RVE sizes. However, the change is lower than 5%. And note that the change could also be influenced by the slight variations in fiber volume fractions between samples.

Based on the analysis, all three RVE sizes appear to be suitable for a uni-directional fiber orientation case. Considering the computational cost associated with these sizes are still manageable, RVE size of 4L6D is selected for the uni-directional fiber orientation sample to achieve maximum accuracy.

2.2.2 Planar fiber orientation case

For the planar fiber orientation case, two sizes for the micro-structural samples were examined, namely 2L4D and 3L3D. Similarly to the UD RVEs, 4 realizations were

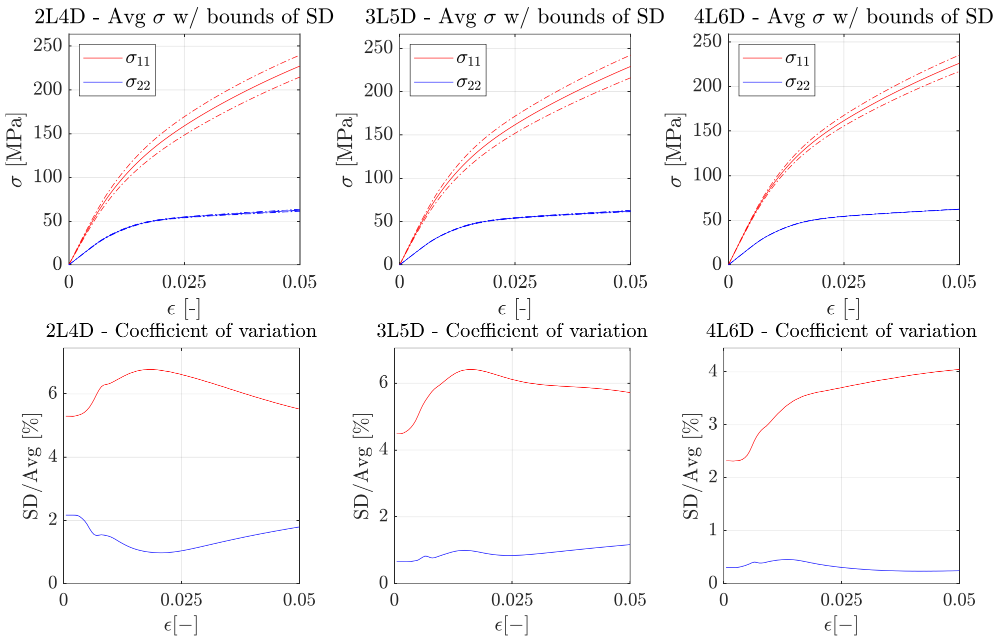

Fig. 2: The average σ_{11}, σ_{22} (top) and coefficient of variation (bottom) results for uni-directional fiber orientation with different RVE sizes. The first, second, and third column correspond to 2L4D, 3L5D, and 4L6D, respectively.

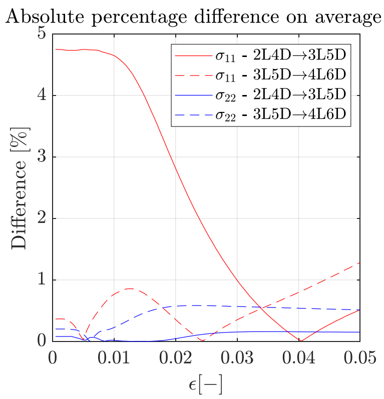

Fig. 3: Absolute percentage different for uni-directional fiber orientation with different RVE sizes.

generated for each size. An attempt is made to generate planar random fiber orientations. Components of the fiber orientation tensor and fiber voluem fractions for different sizes and different relaizations are found in Table 4. Uni-axial stress loading cases, including σ_{11}, σ_{33}, σ_{12} and σ_{13} were tested, using the same loading method as the uni-directional fiber orientation study. Figure 4 shows the average response with

Table 4: List of planar fiber orientation samples properties.

Size	Sample	a_{11}	a_{22}	a_{33}	a_{12}	a_{13}	a_{23}	v_f
2L4D	#1	0.5141	0.4859	0	0.03666	0	0	0.08001
	#2	0.4863	0.5137	0	0.03701	0	0	0.07999
	#3	0.4963	0.5037	0	-0.04389	0	0	0.08000
	#4	0.507	0.493	0	-0.01167	0	0	0.08000
3L3D	#1	0.5003	0.4997	0	-0.04302	0	0	0.08001
	#2	0.5188	0.4812	0	0.09735	0	0	0.08000
	#3	0.5174	0.4826	0	0.05389	0	0	0.08000
	#4	0.516	0.484	0	-0.09783	0	0	0.08000

bounds of standard deviation and the coefficient of variation results for uni-axial stress loading in σ_{11} and σ_{33}. Due to the planar nature of fiber distributions, σ_{11} and σ_{33}

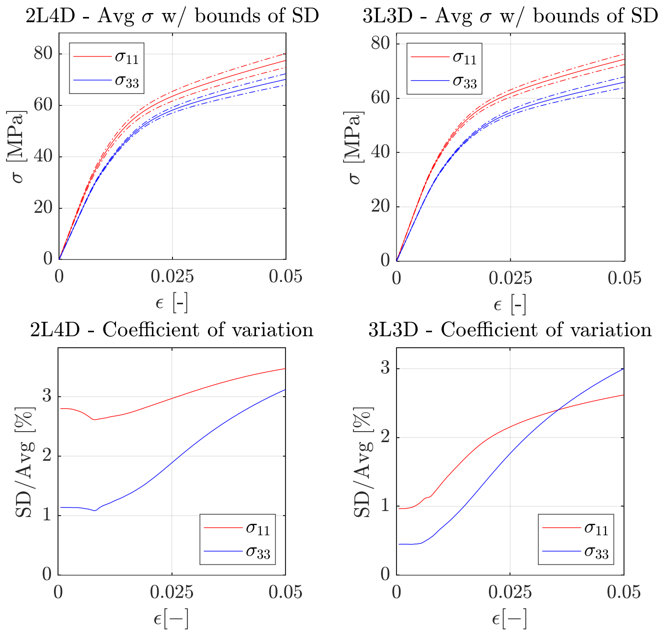

Fig. 4: The average σ_{11}, σ_{33} (top) and coefficient of variation (bottom) results for planar random fiber orientation with different RVE sizes. The first, and second column correspond to 2L4D, and 3L4D, respectively.

components are rather close to each other, as it can be clearly seen in Figure 4. Additionally, it is observed that the variations for the two sizes are lower than 3.5%. Figure 5 illustrates the absolute percentage of difference in average stress for different sizes of the micro-structural samples. The stress component with the highest change is σ_{33}, with a maximum of just below 6%. Considering the low variation observed with the 2L4D size and relatively low changes in average behaviour compared to the 3L3D size,

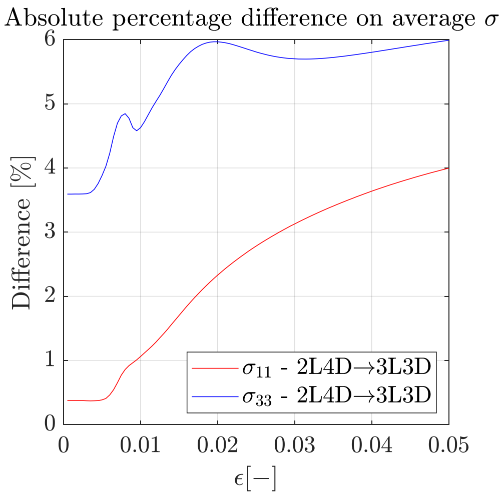

Fig. 5: Absolute percentage different for planar random fiber orientation with different RVE sizes.

using the 2L4D size should be able to provide representative results while still allowing for a manageable computational time. Therefore, an RVE size of 2L4D is selected for the planar fiber orientation sample.

2.3 Finite element and fast Fourier transfer simulations

Finite Element (FE) and Fast Fourier Transfer (FFT) solvers within Digimat-FE were employed to conduct the simulations. The FE solver is used with a conforming mesh, and the FFT solver utilizes a grid. Figure 6 illustrates the different discretization methods. The conforming mesh preserves a higher accuracy of geometrical characteristic of

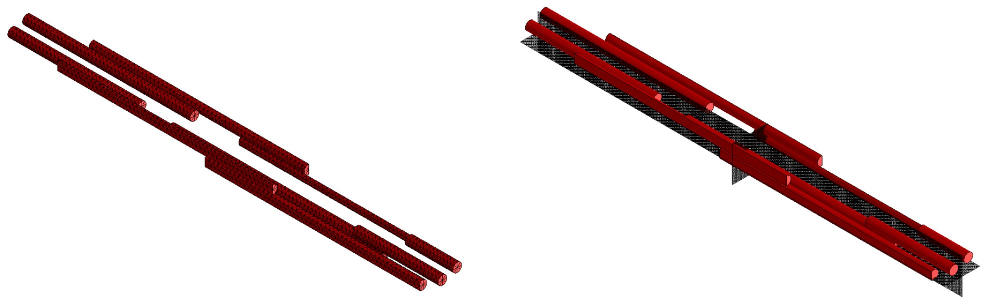

Fig. 6: Fibers spatially discretized using a conforming mesh for the FE solver (left) and the grid used by the FFT solver (right).

the original RVE realization. This results in a more accurate prediction. On the other hand, the FFT solver discretizes the domain using a grid, which may potentially influence the results. Therefore, a comparison between the two solvers is conducted using a 3D RVE subjected to a random strain path. The RVE properties are given in Table 5. Figure 7 shows a comparison of the obtained results using the two methods. Note

Table 5: Properties of a 3D RVE sample used for solver comparison.

Size	a_{11}	a_{22}	$a33$	a_{12}	a_{13}	a_{23}	v_f
1.67L	0.2943	0.3842	0.3215	-0.007636	0.01868	0.03679	0.1111

that the FE analysis was aborted at increment Number 57, while the FFT analysis was able to complete the simulation. It is observed that the stress responses calculated

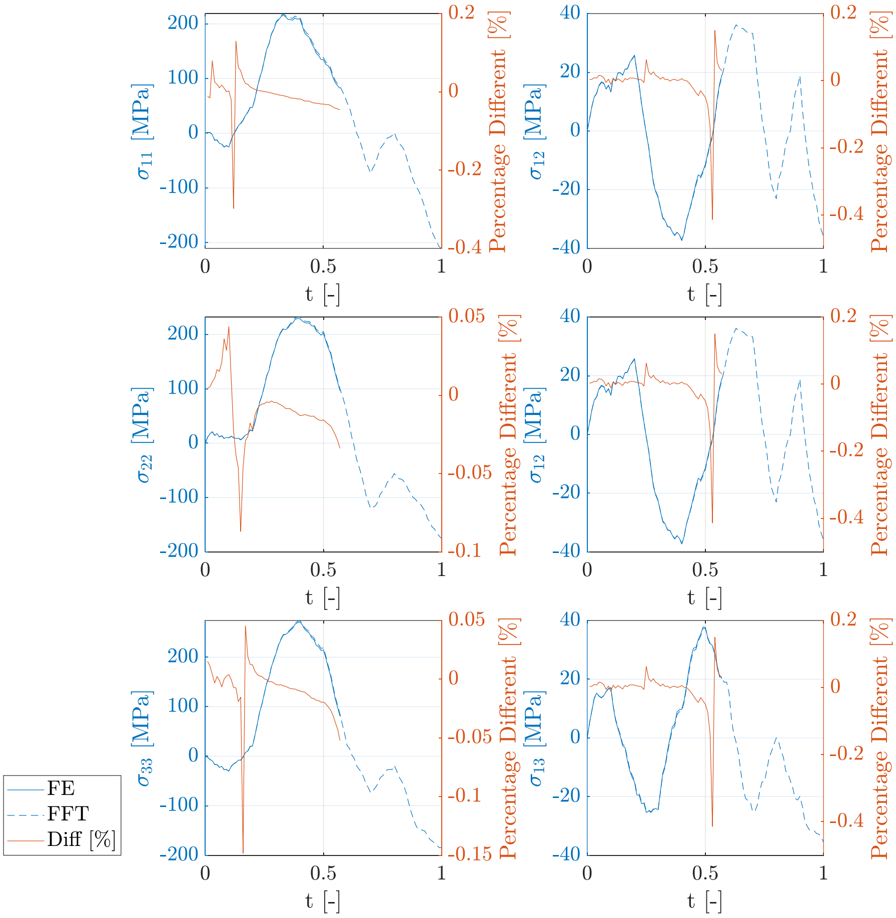

Fig. 7: A comparison of results obtained using FE and FFT methods for a 3D RVE subjected to a random loading path.

from FE and FFT analyses are quite similar. The maximum percentage of the absolute difference between the two approaches is less than 0.5%. Therefore, for the purpose of modeling elasto-plastic response of Short Fiber Reinforced Composites (SFRCs), it is possible to use the FFT approach for accurate high-fidelity full-field simulations.

2.4 Implementation

Table 6 gives the random strain path generation settings. The choice of 100 time

Table 6: Settings used for random strain path generation

Parameter	Distribution	Range/ Value
n − TimeSteps	-	100
n − Drift	uniformly sampled	(1, 2, 5, 10)
γ	uniformly sampled	(0-1)
ε_{max}	uniformly sampled	(0.01-0.05)

steps (n − TimeSteps) was driven by computational requirements of RVE simulations. The number of drift directions (n − Drift) is randomly selected from a set of options, including 1, 2, 5, or 10. As the number of drift directions increases, the complexity of the strain path also increases. However, it also leads to potential issues for convergence in the simulation. Therefore, a maximum of 10 drift directions are selected to balance the complexity and convergence considerations.

2.5 Data post-processing

Table 7 provides the precise number of data in the data set for different orientation cases and solvers.

Table 7: Number of data samples generated to form the full-field data set.

Fiber orientation case	Solver	Train	Valid	Test	Total
UD	FE	14	2	1	17
	FFT	20	4	1	25
Planar	FE	104	20	6	130
	FFT	100	19	6	125
3D	FE	0	0	0	0
	FFT	200	38	12	250
All		438	83	26	547

3 Transfer learning

3.1 General loading test

Five different RVEs were generated from distinct random orientation tensors. Each RVE was subjected to all five general loading cases. The properties of each RVE are presented in Table 8.

Table 8: Properties (components of the orientation distribution tensor and fiber volume fraction) of the general test samples.

Sample	a_{11}	a_{22}	a_{33}	a_{12}	a_{13}	a_{23}	v_f
#1	0.0197	0.4926	0.4877	0.0172	-0.0223	0.2963	0.1152
#2	0.5193	0.3062	0.1745	0.0613	-0.1175	-0.1690	0.1320
#3	0.6291	0.2851	0.0858	0.3868	0.0636	0.0443	0.1409
#4	0.7748	0.0946	0.1306	0.0540	0.1060	-0.0576	0.1142
#5	0.4435	0.2642	0.2923	-0.2709	-0.0629	0.0234	0.1314

3.2 Evaluation procedure

Figure 8 illustrates the procedure of interpolating the input data and removing intermediate predictions.

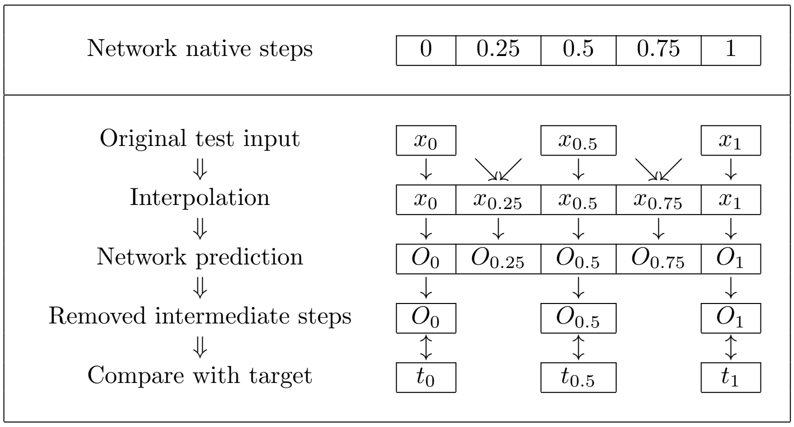

Fig. 8: Illustration of the testing procedure for a network trained with longer time steps compared to the test sample.